Eur. J. Mech. B - Fluids 19 (2000) 285–301

S0997-7546(00)00106-0/FLA

Migrating sea ripples

Paolo Blondeaux [a,*], Enrico Foti [b], Giovanna Vittori [a]

[a] *Dipartimento di Ingegneria Ambientale, Università di Genova, Via Montallegro 1, 16145 Genova, Italy*
[b] *Istituto di Idraulica, Idrologia e Gestione delle Acque, Università di Catania, Viale Andrea Doria 6, 95125 Catania, Italy*

(Received 17 May 1999; revised 11 October 1999; accepted 12 October 1999)

Abstract – Ripple formation under sea waves is investigated by means of a linear stability analysis of a flat sandy bottom subject to the viscous flow which is present in the boundary layer at the bottom of propagating sea waves. Nonlinear terms in the momentum equation are retained to account for the presence of a steady drift. Hence the work by Blondeaux is extended by considering steeper waves and/or less deep waters. Second order effects in the sea wave steepness are found to cause neither destabilizing nor stabilizing effects on the process of ripple formation. However, because of the presence of a steady velocity component in the direction of wave propagation, ripples are found to migrate at a constant rate which is predicted as function of sediment and wave characteristics. The analysis assumes the flow regime in the bottom boundary layer to be laminar and the results are significant for ripples at the initial stage of their formation or for mature ripples of small amplitude (rolling-grain ripples). A comparison of the theoretical findings with laboratory experiments supports the reliability of the approach and of the theoretical results. © 2000 Éditions scientifiques et médicales Elsevier SAS

ripple formation / linear stability analysis / laminar flow

1. Introduction

The ripples which cover the sea bed are usually observed in presence of complex flow fields in which steady as well as periodic components may be present. Therefore coastal ripples are usually classified into three main groups [1]: wave ripples, wave-current ripples and current ripples. Wave ripples are generated by an oscillatory flow characterized by an amplitude much larger than that of the steady component. Wave ripples are periodic ondulations of the sea bed with the crests sharper than the troughs and symmetric with respect to their crests and troughs. Moreover wave ripples are characterized by wavelengths l^* which usually do not exceed a few decimetres and by both small heights h_r^* ($h_r^*/l^* < 0.1$) and large heights ($h_r^*/l^* > 0.1$). In the former case (rolling-grain ripples) the bottom boundary layer keeps attached to the bed profile, while in the latter case (vortex ripples) flow separates at the crests of the bottom waviness and vortex structures are generated. On the other hand when the steady current prevails on the oscillatory motion, current ripples appear which have many characteristics in common with the small bedforms which cover river beds. When the two effects have the same order of magnitude the so-called wave-current ripples are introduced.

The distinguishing geometric feature of wave-current ripples is the asymmetry of their profile. The observation of Inman [2], Inman and Bowen [3], Harms [4], Tanner [5], Tietze [6] (private communication to Allen [7]) indicate that ripples tend to become more asymmetrical as the mass transport velocity increases. Moreover it appears that a unidirectional current unrelated to waves (see the experiments by Inman and Bowen [3] and Harms [4]) affects ripple asymmetry in much the same way as wave-induced mass-transport.

* Correspondence and reprints.

Another aspect which is peculiar of wave-current ripples is their migration in the direction of the steady flow as it appears even from the internal structure of the ripples ([8–10]) as described by Allen [1].

Even though a lot of works have been devoted to the study of ripple formation and development (see the recent contributions by Blondeaux [11], Blondeaux and Vittori [12], Hara and Mei [13,14], Vittori and Blondeaux [15,16], Hara, Mei and Shum [17] and the references therein) because of the practical interest which arises in connection with sand transport in nearshore regions, a lot of them are aimed at the study of wave ripples, i.e. ripples generated by pure oscillatory flows. In this case the mechanics of ripple formation is qualitatively and quantitatively understood. Indeed since the works by Lyne [18] and Sleath [19] appeared, it is known that a small spatially periodic perturbation of the sea bottom under wave action produces steady streamings which consist of recirculating cells, the form, intensity and direction of which depend on the characteristics of the wave and of the perturbation. Because the sediment is driven by the fluid, if the steady drift in the vicinity of the bed is directed from the troughs towards the crests of the perturbation and is strong enough, the latter grows and a pattern of regular or irregular sandy waves appears. A first attempt to quantify the conditions for ripple appearance was performed by Kennedy and Falcon [20]. The idea was further developed by Sleath [19], Blondeaux [11] and Foti and Blondeaux [21] and now the conditions of ripple formation are known. The tendency of sediment to pile up near the crests is opposed by the gravity force acting down the slope of the bed. Hence when nonlinear effects, which become significant for large ripple amplitude, decrease the intensity of the steady drift from the troughs to the crests, the growth of ripple amplitude is inhibited and an equilibrium configuration is reached [15]. For a summary of the results, the interested reader can look at the books of Sleath [22], Fredsøe and Deigaard [23], Nielsen [24] and at the recent review paper by Blondeaux and Vittori [25].

Much less is known on wave-current ripples and current ripples. The interaction of a sea wave with the bottom gives always rise to an oscillatory component plus a steady one, the magnitude of which depends on the wave slope and on the local depth. Sometimes the steady drift is negligible but other times it turns out to be relevant. The present contribution is aimed at the study of ripple formation under sea waves when the wave slope is so large and/or the local depth so small that a uniform steady drift is generated which cannot be neglected when compared with the oscillatory component of the flow. This study is thus a first step towards the investigation of wave-current ripples. At first we wish to investigate whether the steady drift has a stabilizing or a destabilizing effect on the process of ripple formation. Secondly we wish to give an estimate of the propagation velocity of ripples and relate it to the sediment flow rate. This information is of practical interest since it is common practice in the field to evaluate the average sediment transport rate from measurements of ripple migration assuming that the sediment transport rate is related to the migration speed times the height of the ripples [23]. However this holds only when sediment motion in the troughs of the ripples is negligible, i.e. for large amplitude ripples.

Because, to the authors' knowledge, there is a paucity of data concerning ripple characteristics (in particular their migration speed) when the steady uniform velocity component induced by propagating waves assumes significant values, a preliminary experimental investigation of the phenomenon was carried out during which the ripple migration speed was measured. The results obtained, along with the experimental procedure are summarized in Appendix A. The experimental data are compared with the theoretical findings which are obtained by means of a linear stability analysis of a flat sandy bottom subject to a propagating sea wave where second order effects in the wave slope are retained to account for the steady drift. The analytical solution by Vittori and Blondeaux [26] for the viscous flow generated by a propagating wave over a wavy bottom is used. Hence the flow regime is supposed to be laminar. The results outlined in [27] and [25] show that the wave induced flow may remain laminar over a wide range of field conditions and the laminar flow results may still be a reasonable first approximation for moderate values of the Reynolds number when turbulence appears only during decelerating phases. Moreover the grain size should be assumed to be much smaller than the thickness

of the bottom boundary layer because the experimental observations by Sleath [28] indicate that, even for small values of the Reynolds number, the vortex structures generated by flow separation behind sand grains produce an increased vertical mixing which modifies the laminar solution over a smooth bed in a layer the thickness of which scales with the grain size. A modified version of the sediment flow rate formula proposed by Grass and Ayoub [29] is employed along with the sediment continuity (Exner) equation to predict bottom time development. The conditions for the decay or the amplification of a small sinusoidal perturbation of the bottom are determined and the wavelength of the most unstable disturbance is obtained along with its migration speed. Changes of order a^*/L^* with respect to the results by Blondeaux [11] are found.

The structure of the rest of the paper is the following. In the next section we formulate the theoretical problem and describe its solution. The results are discussed in Section 3. Some conclusions are drawn in Section 4. Finally, in Appendix A, the results of a preliminary experimental investigation of the phenomenon are briefly outlined.

2. The analysis

As described by Vittori and Blondeaux [26] (hereinafter referred to as VB), let us consider a two-dimensional gravity wave of small amplitude a^* (slowly varying in the direction of wave propagation because of viscous damping), length L^* and period T^*, propagating over an initially flat non-cohesive bottom formed by sediments of uniform size d^*, density ρ_s and porosity n (see *figure 1*). At this stage it is worth pointing out that bed porosity will be considered when studying the time development of the bottom configuration induced by the convergence or divergence of the sediments moved by fluid flow, but it will be neglected in the hydrodynamic problem; i.e. the vanishing of the fluid velocity will be forced at the bottom surface, because the water flows through the sediments with a quite small velocity. Let us denote by h^* the constant value of the local depth and by ρ, ν the density and kinematic viscosity of water respectively. In this paper we adopt the notation and definitions of VB; hence a cartesian coordinate system is introduced with the x^*-axis in the direction of wave propagation, lying on the bottom and pointing offshore, and the y^*-axis vertical and pointing upwards. As discussed in VB, the flow field induced by the propagating wave can be divided into three regions: a core region where y^* assumes values of order h^*, a viscous layer adjacent to the bottom the thickness of which is of order $\delta^* = \sqrt{2\nu/\omega^*}$ ($\omega^* = 2\pi/T^*$ being the angular frequency of the sea wave) and a surface layer. Since we are interested in the interaction between fluid and sediments, let us focus our attention on the bottom layer. If the bottom is flat, the flow close to the bed can be easily determined when the wave slope is much smaller than one. In particular in VB it is assumed that the ratio between δ^* and a^* assumes finite values and both the

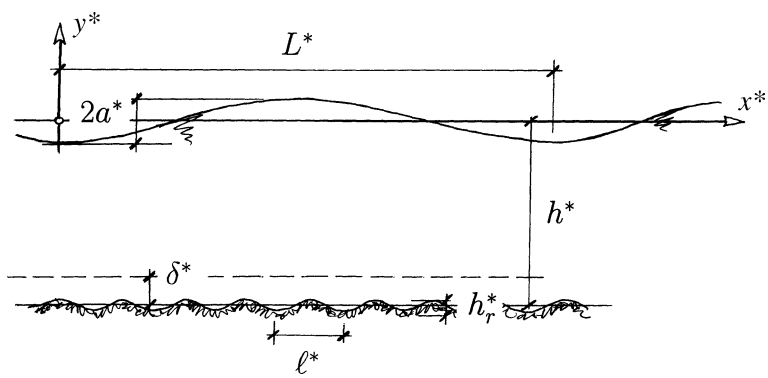

Figure 1. Sketch of the problem.

Table I. Order of magnitude of the length scales involved in the problem.

Water depth	$\sim 10^1$ m
Length of the sea wave	$\sim 10^2$ m
Amplitude of the sea wave	$\sim 10^0$ m
Thickness of the viscous bottom boundary layer	$\sim 10^{-3}$–10^{-2} m
Length of ripples	$\sim 10^{-1}$ m
Amplitude of ripples at regime	$\sim 10^{-2}$ m

quantities are much smaller than L^*. The assumption that the ratio δ^*/a^* assumes finite values might appear restrictive. However defining the Reynolds number of the bottom boundary layer as

$$Re = \frac{U_0^*\delta^*}{\nu} = \frac{2}{\delta}\frac{a^*}{L^*\sinh[2\pi h^*/L^*]}, \tag{1}$$

where δ is δ^*/L^* and $U^* = a^*\omega^*/\sinh[2\pi h^*/L^*] = a^*\omega^*/S$ is the amplitude of the irrotational velocity oscillations close to the bottom, it can be easily verified that

$$\frac{a^*}{L^*} = \frac{\delta^*}{L^*}Re\frac{\sinh(2\pi h^*/L^*)}{2} \tag{2}$$

and

$$\frac{a^*}{\delta^*} = Re\frac{\sinh(2\pi h^*/L^*)}{2}. \tag{3}$$

Hence the assumption $\delta = \delta^*/L^* \ll 1$ simply implies $a^*/L^* \ll 1$ which is an hypothesis usually employed studying sea waves. The assumption that the ratio a^*/δ^* is neither infinite small nor infinite large, but it can assume only finite values (not necessarily close to one), has been made to avoid the introduction of a further unnecessary perturbative parameter (namely Re). It is worth pointing out that we performed computations with values of Re up to 100 which are typical values of the Reynolds number for bottom boundary layers in the laminar regime. (Sometimes the Reynolds number $RE = U_0^*(U_0^*/\omega^*)/\nu$ is introduced to characterize the bottom boundary layer. It can be easily verified that $RE = Re^2/2$). Therefore the values of a^*/δ^* considered in paper are similar to those encountered in the field. The assumption $\delta^* \sim a^*$ has been also used by Wen and Liu [30] in a similar context.

In *table I* the order of magnitude of the different length scales involved in the problem is specified for a better understanding of the analysis.

In VB it is then shown that the dimensionless velocity components $(u, v) = (u^*, v^*)/(a^*\omega^*/\sinh[2\pi h^*/L^*])$ turn out to have a part of order one and a part of order δ

$$(u, v) = (u_{00}, v_{00}) + \delta(u_{10}, v_{10}) + \mathrm{O}(\delta^2). \tag{4}$$

The detailed form of $u_{00}, v_{00}, u_{10}, v_{10}$ as function of $t = \omega^* t^*$ and $(\tilde{x}, \tilde{y}) = (x^*, y^*)/\delta^*$ is obtained in VB, where it is shown that the velocity components depend also on the Reynolds number Re of the bottom layer. For sake of completeness, we provide the reader the functions appearing in (4):

$$u_{00} = \hat{u}_{00}(\tilde{y})\mathrm{e}^{i(t+2\pi\delta\tilde{x})} + \text{c.c.} = -\frac{1}{2}\left[1 - \mathrm{e}^{-(1+i)\tilde{y}}\right]\mathrm{e}^{i(t+2\pi\delta\tilde{x})} + \text{c.c.}, \tag{5}$$

$$v_{00} \equiv 0, \tag{6}$$

$$u_{10} = \left[\bar{u}_{10}(\tilde{y}) + \hat{u}_{10}(\tilde{y})\mathrm{e}^{2i(t+2\pi\delta\tilde{x})}\right] + \text{c.c.}, \tag{7}$$

where

$$\bar{u}_{10} = -\frac{\pi Re}{4}\left\{\frac{3}{2} + \frac{1}{2}\mathrm{e}^{-2\tilde{y}} - \mathrm{e}^{-(1-i)\tilde{y}}\left[2 + i + (1-i)\tilde{y}\right]\right\}, \tag{8}$$

$$\hat{u}_{10} = 2iC_1 - \frac{\pi Re}{4}\mathrm{e}^{-(1+i)\tilde{y}}\left[1 - (1+i)\tilde{y}\right] + \mathrm{e}^{-\sqrt{2}(1+i)\tilde{y}}\left[\frac{\pi Re}{4} - 2iC_1\right], \tag{9}$$

$$C_1 = \frac{3}{16}\pi i Re\left[\cosh(4\pi h^*/L^*) - \frac{\sinh(4\pi h^*/L^*)}{2\tanh(2\pi h^*/L^*)}\right]^{-1} \tag{10}$$

and

$$v_{10} = \hat{v}_{10}(y)\mathrm{e}^{i\tilde{t}} + \text{c.c.} = \pi i\left[\tilde{y} + \frac{1}{1+i}\left(\mathrm{e}^{-(1+i)\tilde{y}} - 1\right)\right]\mathrm{e}^{i(t+2\pi\delta\tilde{x})} + \text{c.c.} \tag{11}$$

In (5)–(11) c.c. denotes the complex conjugate of a complex quantity. It is worth pointing out that (8) is the Eulerian steady velocity component predicted by Longuet-Higgins [31]. In order to ascertain whether the initially plane bottom keeps flat under the action of the sea wave, it is necessary to quantify the sediment motion induced by the fluid flow and to determine the changes in bottom elevation due to erosion and deposition processes. Bottom time development is controlled by the sediment continuity equation together with a relationship between sediment flow rate per unit width q^* and flow properties. As discussed in [11], a relationship can be simply obtained by relating q^* to the agitating forces which act on sediment grains. The sediments move subject to the drag force and to the gravity component along the bed profile, other forces being negligible. Following an approach which is widely used in research on steady sediment transport [32], but which can be applied also to unsteady flows, the sediment transport rate can be assumed to be proportional to some power b of the agitating forces. Here the drag force is assumed proportional to $\mu V^* d^*$ and the gravity component along the bed profile to $(\rho_s - \rho)gd^{*3}(\partial\eta^*/\partial x^*)$ (η^* being the bed surface elevation, V^* fluid velocity parallel to the bottom profile evaluated at $y^* = \eta^* + \frac{1}{2}d^*$ and μ the dynamic viscosity of the fluid). To quantify the drag force acting on sediment grains the fluid velocity at $d^*/2$ is used because this value leads to a predicted sediment transport rate which is in-phase with Sleath's [33] measurements, the only ones describing the time development of q^*. Hence in a dimensionless form we can write

$$q = \hat{a}\left|\frac{2}{R_d}V - \frac{\beta}{\psi}\frac{\partial\eta}{\partial\tilde{x}}\right|^b_{\tilde{y}=\eta+d/2}\operatorname{sgn}\left(\frac{2}{R_d}V - \frac{\beta}{\psi}\frac{\partial\eta}{\partial\tilde{x}}\right)_{\tilde{y}=\eta+d/2}, \tag{12}$$

where $q = q^*/\sqrt{[(\rho_s/\rho) - 1]gd^{*3}}$, $V = V^*/(a_0^*\omega^*/\sinh[2\pi h^*/L^*])$ and $d = d^*/\delta^*$. In (12) the parameters particle Reynolds number R_d, mobility number ψ and the ratio between sediment and fluid densities s are defined in the form

$$\psi = \frac{(U_0^*)^2}{(s-1)gd^*}, \qquad R_d = \frac{U_0^* d^*}{\nu}, \qquad s = \frac{\rho_s}{\rho}. \tag{13}$$

The constant β in (12), introduced following Fredsøe [34] who suggested a value ranging between 0.1 and 1, will be assumed equal to 0.15 as in [11]. The values of $\hat{a}$ and b can be estimated in the relevant range of the parameters (i.e. for $d^* < \delta^*$) for example by requiring that relationship (12) should match the empirical law proposed by Grass and Ayoub [29]. In this way it is found that $\hat{a}$ is function of s, R_d and ψ ($\hat{a} = 1.23((s-1)/s)\psi^{3.36}R_d^{1.83}$) and b is equal to 4.28. Other empirical formulae can be used to evaluate $\hat{a}$ as described in Section 3, where the theoretical findings are compared with the experimental data described in Appendix A. Two points need to be addressed in discussing the reliability of the sediment transport rate formula: (1) the qualitative time behaviour of the sediment transport rate q^*; (2) the amount of sediment moved by the

fluid which can be quantified by $\overline{q^*}$, i.e. by the value of q^* averaged over that half of the wave cycle, during which sediment transport does not change direction. Needless to say, at the leading order of approximation, the flow is assumed to be symmetric and the averaged sediment transport rate in the offshore direction equals that in the onshore direction.

The qualitative time behaviour of the sediment transport rate described by (12) fairly agrees with the data described in [33] and with the empirical law he proposed. Indeed Sleath [33] indicated that the quantity of sediment particles swept off the bed and carried by the flow is proportional to the fourth power of the fluid velocity outside the bottom boundary layer when an appropriate phase lead is introduced which depends on the grain size. The value adopted for b is close to 4 and a comparison between (12) and the data by Sleath [33] shows that the time delay between the irrotational velocity oscillations and those of the sediment transport rate is well predicted by introducing in (12) the fluid velocity V^* evaluated at $y^* = \eta^* + d^*/2$. The lack in (12) of any threshold condition for sediment motion is justified by the experimental observation that, whenever the actual values of the parameters are beyond the critical values corresponding to the threshold condition for sediment motion [22], moving particles are always present and during the portion of the cycle when almost all sediment grains are at rest, the sediment transport rate predicted by (12) practically vanishes.

The predictions of the amount of sediment moved by the flow are not in agreement with the measurements by Sleath [33] and with the empirical relationship he proposed [33]. However it should be pointed out that later Sleath [22] himself stated that the law proposed by Sleath [33] cannot be applied for small grain sizes, since it is based on data obtained using large grain sizes. Most importantly it is worth pointing out that the results described in the present paper are not affected by the value of $\hat{a}$ but only on the dependence of q^* on t^*, i.e. on the value of b.

Since the bottom profile is described by

$$y^* = \eta^*(x^*, t^*) \tag{14}$$

the dimensionless form of sediment continuity equation turns out to be [34]

$$-\frac{2\sqrt{\psi}}{R_d}(1-n)\frac{\partial \eta}{\partial \tilde{t}} = \frac{\partial q}{\partial \tilde{x}} + 2\pi\delta\frac{\partial q}{\partial \tilde{t}}, \tag{15}$$

where n is the bed porosity and the variable $\tilde{t}$ has been introduced to reduce the amount of algebra which is necessary to find the solution,

$$\tilde{t} = t + 2\pi\delta\tilde{x}. \tag{16}$$

Equation (15) simply states that changes in bottom elevation are due to the spatial variations of the sediment transport rate which take place on a scale equal to the boundary layer thickness and are induced by the bottom waviness (first term on the right hand side of (15)) plus those induced by the propagation of the surface wave (second term on the right hand side of (15)). However the latter are much smaller than the former since they take place on much longer spatial scales ($O(L^*)$). In order to determine bottom time development, it is more convenient to write equation (15) in the form

$$\frac{\partial \eta}{\partial \tilde{t}} = -Q\left[\frac{\partial \tilde{q}}{\partial \tilde{x}} + 2\pi\delta\frac{\partial \tilde{q}}{\partial \tilde{t}}\right], \tag{17}$$

where $\tilde{q}$ turns out to be a function of order one and the parameter Q, for sand under wind waves, is much smaller than one

$$\tilde{q} = \left|2\frac{Re}{R_d}V - \frac{\beta Re}{\psi}\frac{\partial \eta}{\partial \tilde{x}}\right|_{\tilde{y}=d/2}^{b-1}\left(2\frac{Re}{R_d}V - \frac{\beta Re}{\psi}\frac{\partial \eta}{\partial \tilde{x}}\right)_{\tilde{y}=d/2}, \tag{18}$$

$$Q = \frac{\hat{a}R_d}{2(1-n)\sqrt{\psi}Re^b} \ll 1. \tag{19}$$

Indeed it is easy to verify that, when d^* is smaller than δ^*, the dimensionless form V of V^* turns out to be of order d^*/δ^*, i.e. $O(R_d/Re)$. Because of the presence of the small parameter Q, equation (17) suggests that even when $\partial\tilde{q}/\partial\tilde{x}$ is of order one, bottom changes are quite small, i.e. of $O(Q)$ or take place on a slow morphological time scale $\tau = Q\tilde{t}$. Therefore the flow field can be computed on a fixed bottom configuration or on a parametrically varying bottom profile, if terms of order Q are neglected.

Since the sea wave which propagates on a flat bottom is characterized by no spatial dependence on the fast variable $\tilde{x}$ but only on the slow variable $x = \delta^*\tilde{x}/L^*$, $\partial\tilde{q}/\partial\tilde{x}$ turns out to vanish and bottom changes are of order δQ. At the leading order of approximation, it is thus possible to assume

$$\eta = \delta Q \eta_0. \tag{20}$$

Equation (20) leads to the conclusion that (4) along with the relationships for $u_{00}, v_{00}, u_{10}, v_{10}$ given in VB can be assumed valid even in the non-cohesive bottom case, if terms of order δQ can be neglected in the velocity field.

By solving (17) at the leading order of approximation, it is possible to obtain

$$\eta_0 = -2\pi\left|2\frac{Re}{R_d}u_{00}\right|_{\tilde{y}=d/2}^{b-1}\left(2\frac{Re}{R_d}u_{00}\right)_{\tilde{y}=d/2}, \tag{21}$$

where u_{00} is provided by (5). Equations (20) and (21) describe a sandy wave the amplitude of which is of $O((\delta^*)^2 Q/L^*)$, the wavelength being L^*.

Even though field surveys do not show the presence of a sandy wave induced by the propagating sea wave, its existence cannot be questioned since sediment transport at the bottom of sea waves is commonly observed in the same direction as wave propagation in front of the crests and in the opposite direction in front of the troughs. These observations lead to the conclusion that sediments are piled up behind wave troughs while they are swept away behind the crests generating a wavy bottom. No sand wave with the same period and wavelength of the water wave has ever been observed in the field because of the slow spatial variations of q^* and the high frequency of water waves. Indeed the order of magnitude of the amplitude of this sandy wave can be estimated by using sediment continuity equation [23] and it turns out to be

$$\overline{q^*}T^*/L^*, \tag{22}$$

where $\overline{q^*}$ is the sediment transport rate averaged over half a cycle previously defined and T^*, L^* are the period and wavelength of the surface gravity wave. Whatever formula is used to compute $\overline{q^*}$, the amplitude of the sandy wave turns out to be many orders of magnitude smaller than the size of the sand grains.

We are now wondering whether the bottom configuration (20) is stable or unstable with respect to perturbations of small amplitude $\epsilon\delta^*$ ($\epsilon \ll 1$) and length scale δ^*. In other words we want to determine the time development of a perturbation $\epsilon\eta_1(\tilde{x}, \tilde{t})$ superimposed to (20)

$$\eta = \delta Q \eta_0 + \epsilon\eta_1(\tilde{x}, \tilde{t}). \tag{23}$$

Since for sand and wind waves Q is of order 10^{-3} and δ is of order 10^{-5}, it is possible and reasonable to consider situations such that

$$\delta Q \ll \epsilon \ll 1. \tag{24}$$

Therefore our attention will be focused on bottom perturbations of initially small amplitude with respect to δ^* but larger than the amplitude $(\delta Q)\delta^*$ of the sandy wave produced by the propagation of the sea surface wave over the non-cohesive bottom.

Assumption (24) does not limit the analysis too much, since in the field δQ assumes quite small values. Some limitations to the applicability of the results to field situations came from the other assumptions already introduced, i.e. (1) waves of small amplitude $(a^*/L^* \ll 1)$; (2) laminar regime in the bottom boundary layer (Re smaller than a critical value which ranges between 100 and 500; see [25,27]). However assumption (1) is commonly used in the studies of sea wave propagation as well as assumption (2) is often introduced in the theoretical attempts to understand ripple formation and development ([11,13,14,19,35]).

Because of the assumption of a small amplitude perturbation, it is feasible to perform a normal mode analysis and consider a bottom perturbation in the form

$$\epsilon\eta_1(\tilde{x}, \tilde{t}) = \epsilon C(\tilde{t})\mathrm{e}^{i\alpha\tilde{x}} + \text{c.c.}, \tag{25}$$

where c.c. denotes the complex conjugate of the foregoing term and $C(\tilde{t}), \alpha$ are the amplitude and the wavenumber of the generic perturbation component, respectively. The results will show that the growth or the decay of the amplitude $C(\tilde{t})$ strongly depends on the value of α. In particular, when the parameters of the problem are such that the flat bottom configuration turns out to be unstable, a sinusoidal component of wavenumber α_M can be identified which is characterized by the maximum growth rate. In the framework of the linear approach presently employed, it can be concluded that for long times such perturbation component will prevail and will originate a bottom waviness characterized by a dimensionless wavelength equal to $2\pi/\alpha_M$.

As previously discussed, the sediment continuity equation (17) shows that bottom changes which take place on the fast time scale $\tilde{t}$ are of order Q. Hence if $\mathrm{O}(Q)$ terms are neglected in the flow field, the velocity produced by the propagation of the surface wave over the bottom described by (21) and (22) turns out to be

$$\begin{aligned}(u, v) = (u_{00}, v_{00}) + \delta(u_{10}, v_{10}) + \epsilon\big\{C(\tilde{t})\big[(\hat{u}_{01}, \hat{v}_{01})\\ + \delta(\hat{u}_{11}, \hat{v}_{11})\big]\mathrm{e}^{i\alpha\tilde{x}} + \text{c.c.}\big\} + \mathrm{O}\big(\delta^2, \epsilon^2, Q\big).\end{aligned} \tag{26}$$

The functions $\hat{u}_{01}, \hat{v}_{01}, \hat{u}_{11}, \hat{v}_{11}$ can be written in the form

$$\big(\hat{u}_{n1}, \hat{v}_{n1}\big) = \sum_{m=-\infty}^{\infty} \big(u_{n1}^{(m)}(\tilde{y}), v_{n1}^{(m)}(\tilde{y})\big)\mathrm{e}^{im\tilde{t}} \quad (n = 0, 1) \tag{27}$$

which, along with (26), show the existence of spatially periodic recirculating cells oscillating in time. As described in VB the unknown functions $(u_{n1}^{(m)}, v_{n1}^{(m)})$ can be found by solving systems of coupled ordinary differential equations by a shooting method. In particular the non-vanishing values of $(u_{n1}^{(0)}, v_{n1}^{(0)})$ indicate the existence of steady streamings which play a fundamental role in the growth of the bottom perturbations. Because of the presence of $u_{11}^{(0)}$ and $v_{11}^{(0)}$ these steady streamings are no longer symmetric with respect to ripple crests and troughs as found in [11] and thus they induce, as discussed later, ripple migration. The reader interested in a discussion of the behaviour of $(u_{n1}^{(m)}, v_{n1}^{(m)})$ is referred to VB.

Equation (18) leads to the following form of the sediment flow rate

$$\tilde{q} = (\tilde{q}_{00} + \delta\tilde{q}_{10}) + \big[\epsilon C(\tilde{t})(\tilde{q}_{01} + \delta\tilde{q}_{11})\mathrm{e}^{i\alpha\tilde{x}} + \text{c.c.}\big] + \mathrm{O}\big(\delta^2, \epsilon^2, Q\big), \tag{28}$$

where $\tilde{q}_{00}, \tilde{q}_{10}, \tilde{q}_{01}$ and $\tilde{q}_{11}$ are provided by

$$\tilde{q}_{00} = \left(\frac{2Re}{R_d}\right)^b |u_{00}|^{b-1} u_{00} \quad \text{at } \tilde{y} = d/2, \tag{29}$$

$$\tilde{q}_{10} = \left(\frac{2Re}{R_d}\right)^b b|u_{00}|^{b-1} u_{10} \quad \text{at } \tilde{y} = d/2, \tag{30}$$

$$\tilde{q}_{01} = \left(\frac{2Re}{R_d}\right)^b b|u_{00}|^{b-1}\left(\hat{u}_{01} + \frac{\partial u_{00}}{\partial y} - i\alpha\frac{\beta R_d}{2\psi}\right) \quad \text{at } \tilde{y} = d/2, \tag{31}$$

$$\tilde{q}_{11} = \left(\frac{2Re}{R_d}\right)^b b|u_{00}|^{b-3} u_{00}, \tag{32}$$

$$\left[u_{00}\left(\hat{u}_{11} + \frac{\partial u_{10}}{\partial y} + i\alpha v_{10}\right) + (b-1)u_{10}\left(\hat{u}_{01}\frac{\partial u_{00}}{\partial y} - i\alpha\frac{\beta R_d}{2\psi}\right)\right] \quad \text{at } \tilde{y} = d/2.$$

Moreover the results by Blondeaux [11] indicates that the bottom perturbation beside the fast time scale $\tilde{t}$ depends on a slow time scale $\tau = Q\tilde{t}$ and suggests assuming

$$C(\tilde{t}) = \mathcal{C}(\tau)\left[C_0(\tilde{t}) + QC_1(\tilde{t}) + O(Q^2)\right]. \tag{33}$$

By substituting (25), (28), (33) into (17), at order ϵQ^0 it is easy to obtain

$$\frac{\mathrm{d}C_0}{\mathrm{d}\tilde{t}} = 0.$$

Then C_0 turns out to be equal to a constant which can be set equal to 1 without loss of generality. At order ϵQ equation (17) leads to

$$\mathcal{C}(\tau)\frac{\mathrm{d}C_1}{\mathrm{d}\tilde{t}} + \frac{\mathrm{d}\mathcal{C}}{\mathrm{d}\tau} = -\left[i\alpha(\tilde{q}_{01} + \delta\tilde{q}_{11}) + 2\pi\delta\frac{\mathrm{d}\tilde{q}_{01}}{\mathrm{d}\tilde{t}}\right]\mathcal{C}(\tau) \tag{34}$$

which gives rise to

$$\frac{\mathrm{d}\mathcal{C}}{\mathrm{d}\tau} = \left[-\frac{\mathrm{d}C_1}{\mathrm{d}\tilde{t}} + G(\tilde{t})\right]\mathcal{C}(\tau). \tag{35}$$

It is worth pointing out that considering $\mathrm{O}(Q)$ terms in (33) while neglecting them in the flow field is consistent since the neglected terms in the velocity components would induce effects of $\mathrm{O}(Q^2)$ in (33). The function $G(\tilde{t})$ is a periodic function with a non vanishing time average $\overline{G}$ (hereinafter an overbar denotes the time average over the wave cycle)

$$G(\tilde{t}) = -i\alpha\tilde{q}_{01} - \delta\left[i\alpha\tilde{q}_{11} + 2\pi\frac{\mathrm{d}\tilde{q}_{01}}{\mathrm{d}\tilde{t}}\right] = \overline{G} + \widehat{G}(\tilde{t}). \tag{36}$$

From (35) two equations are obtained

$$\frac{\mathrm{d}C_1}{\mathrm{d}\tilde{t}} = \widehat{G}(\tilde{t}), \tag{37}$$

$$\frac{\mathrm{d}\mathcal{C}}{\mathrm{d}\tau} = \overline{G}\mathcal{C}(\tau). \tag{38}$$

The function $C_1(\tilde{t})$ turns out to be equal to $\int \widehat{G}(\tilde{t})\,\mathrm{d}\tilde{t}$ and describes the small periodic variations of the perturbation profile during a wave cycle. More precisely the real part describes oscillations of the amplitude of

the bottom perturbation while the imaginary part controls the small longitudinal oscillations of the ripple profile around its average position. The growth of the perturbation and consequently ripple formation is controlled by $\overline{G}$:

$$\mathcal{C}(\tau) = \mathcal{C}_0 \exp[\overline{G}\tau]. \tag{39}$$

By its definition, it turns out that $\overline{G}$ is composed of two parts: one of order one and the other of order δ

$$\overline{G} = \overline{G}_0 + \delta\overline{G}_1 \tag{40}$$

with $\overline{G}_0 = \overline{-i\alpha\tilde{q}_{01}}$ and $\overline{G}_1 = \overline{-i\alpha\tilde{q}_{11}}$ ($\overline{2\pi\, \mathrm{d}\tilde{q}_{01}/\mathrm{d}\tilde{t}}$ turns out to be zero because $\tilde{q}_{01}$ is a periodic function of $\tilde{t}$). The former part ($\overline{G}_0$) is coincident with the amplification rate found by Blondeaux [11]. The presence of $\overline{G}_1$ is the main novelty of the analysis: $\overline{G}_1$ is complex and may have both a real and an imaginary part. The real part is the correction of the amplification rate determined by Blondeaux [11] due to second order effects in the wave slope. When the parameters lead to a positive value of $\overline{G}_{1r}$ (the real part of $\overline{G}_1$), it can be stated that nonlinear effects in the wave slope have a destabilizing effect on ripple formation. On the other hand when $\overline{G}_{1r}$ is negative a stabilizing effect is found. The imaginary part ($\overline{G}_{1i}$) of $\overline{G}_1$ controls the propagation speed of the ripple. Indeed, while the imaginary part of $\overline{G}_0$ vanishes because of the symmetry of the problem at the leading order of approximation, $\overline{G}_{1i}$ is different from zero due to the steady Eulerian drift of $0(\delta)$ at the bottom of sea waves.

3. The results

An example of the results is shown in *figure 2* where the values of $\overline{G}_{0r}$ and $\overline{G}_{1i}$ are plotted versus α for fixed values of Re, R_d and different values of ψ. Moreover the parameters s, n, β have been given the following values: 2.65, 0.45, 0.15 respectively. In obtaining the results plotted in *figure 2* and those shown in *figures 3, 4* and *5*, the numerical problems found by VB in computing $\bar{u}_M$ have not been encountered since to evaluate $\overline{G}_0$ and $\overline{G}_1$ only $u_{00}, u_{10}, v_{10}, \hat{u}_{01}, \hat{v}_{01}, \hat{u}_{11}, \hat{v}_{11}$ are required. Hence results can be easily obtained when α ranges between (0.05, 0.5) and Re assumes values up to 100 and even larger. The results of *figure 2(a)* are coincident with those described in [11] when the different definition of the constant Q is taken into account. *Figure 2(a)*, where $O(\delta)$ effects are not included, shows the existence of a critical value ψ_c of ψ such that for ψ less than ψ_c, bottom perturbations decay for each value of the wavenumber α. On the other side for ψ larger than ψ_c bottom perturbations characterized by values of α falling in a restricted range around α_c, experience an average amplification within a cycle. In this case ψ_c is around 2.99. Moreover it has been found that the presence of a steady drift of order δ has neither stabilizing nor destabilizing effects on the process of ripple formation since the real part $\overline{G}_{1r}$ of $\overline{G}_1$ turns out to vanish. The real part of $\overline{G}_1$ has been found to vanish even when different values of Re and R_d are considered. Hence the results described in [11], concerning the critical values of ψ and α, are not changed by $O(\delta)$ effects and their description will not be reported here for sake of brevity. It is worth pointing out that in [11] the results are discussed in terms of a sediment Froude number F_d defined as $\sqrt{\psi}$. The results of *figure 2(b)* indicate that the growth of bottom perturbations takes place simultaneously with their migration in the onshore direction. In fact the imaginary part of $\overline{G}_1$ turns out to be positive whatever value of α is considered (we remind the reader that the x-axis points offshore). Let us now discuss the behaviour of $\overline{G}_{1i}$. Its value is shown in *figure 3* as a function of α for different values of R_d and fixing Re equal to 10 and 30. *Figure 4* shows $\overline{G}_{1i}$ as function of Re for different values of R_d and fixing $\alpha = 0.3$. It is worth pointing out that $\overline{G}_{1i}$ does not depend on the value of ψ since the time average of $u_{10}u_{00}|u_{00}|^{b-3}$ is always zero. In all cases $\overline{G}_{1i}$ turns out to be positive thus indicating that the steady drift at the bottom of sea waves tends to drag the ripples which therefore migrate in the onshore direction. Of course larger values of Re imply

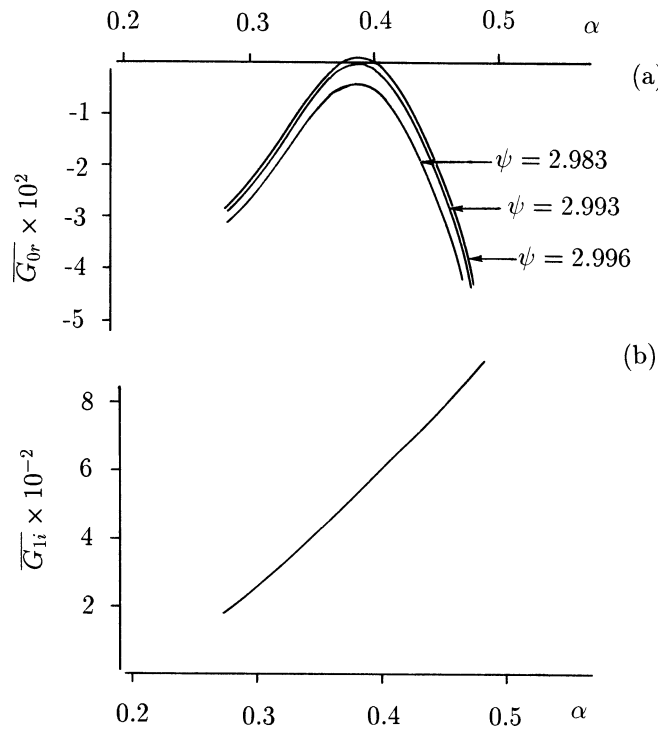

Figure 2. Real part of $\overline{G}_0$ and imaginary part of $\overline{G}_1$ plotted versus α for different values of ψ and for $Re = 35$, $R_d = 10$.

stronger steady currents and hence larger migration speed. The strong increase of $\overline{G}_{1i}$, which is found as α is increased, could less easily be guessed, even though ripple steepness increases as α is increased and hence the drag force is expected to increase too. The theoretical values of $\overline{G}_{1i}(\alpha_c)/\alpha_c$ are plotted in *figure 5* as function of *Re* for different values of R_d along with the experimental values described in Appendix A. Data of other authors, for example those by Inman and Bowen [3] and Gray et al. [36] have not been considered because in many experiments the steady velocity component was due to the superposition of a current unrelated to waves. Moreover in the recent experiments by Gray et al. [36] ripples were generated by random waves.

Since at the leading order of approximation the bottom profile can be written in the form

$$\eta \cong \epsilon \exp[\overline{G}_0 Q\tilde{t}] \exp\left[i\alpha\left(\tilde{x} + \frac{\overline{G}_{1i}}{\alpha}\delta Q\tilde{t}\right)\right]$$
$$= \epsilon \exp\left[\text{Real}(\overline{G}_0) Q\tilde{t}\right] \exp\left[\frac{i\alpha}{\delta^*}\left(x^* + U_0^* \frac{\overline{G}_{1i}}{\alpha} \frac{2\delta Q}{Re} t^*\right)\right] \tag{41}$$

the quantity $\overline{G}_{1i}/\alpha$ is simply the dimensionless migration speed of ripples divided by the factor $(2\delta Q/Re)$. While the theory provides directly the ratio $\overline{G}_{1i}/\alpha$, in order to obtain the experimental points, it is necessary to estimate the constant Q which is related to the amount of sediment moved by the flow averaged during half a cycle. Because in the experiments we performed, the grain size was not much smaller than the bottom boundary thickness, the values of Q provided by (19) with $\hat{a}$ equal to $1.23\,((s-1)/s)\psi^{3.36}R_d^{1.83}$ are not reliable. Indeed the former expression of $\hat{a}$ has been obtained by assuming d^* much smaller than δ^*. Hence to obtain more appropriate values of $\hat{a}$ (and then of Q) we force the time average over half a cycle of (12) to be equal to the value of $\overline{q^*}$ estimated using the formulae suggested by Hallermeier [37] (*figure 5(a)*) and Sleath [22] (*figure 5(b)*) which are supposed to provide reliable predictions of $\overline{q^*}$ for any value of d^*. Hallermeier [37],

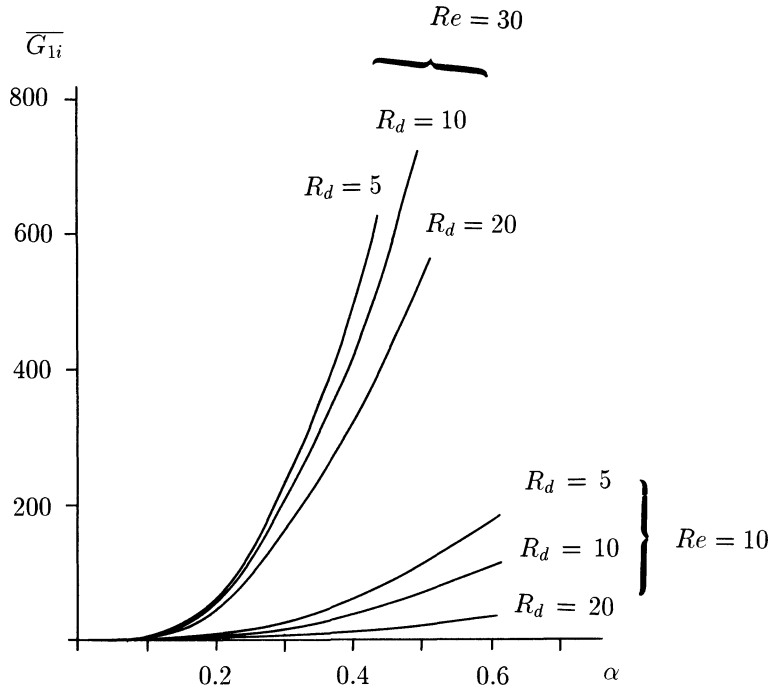

Figure 3. Imaginary part of $\overline{G}_1$ plotted versus α for different values of R_d and $Re = 10,\ 30$.

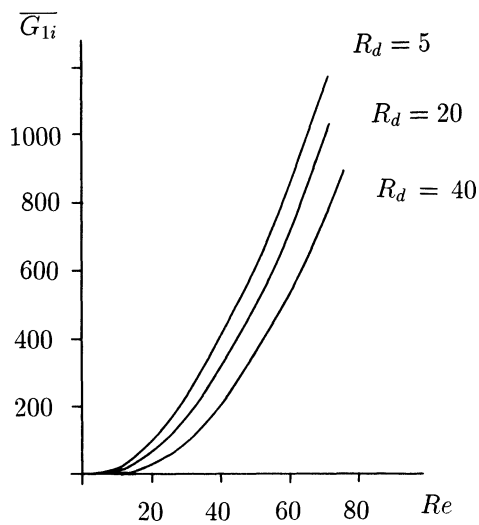

Figure 4. Imaginary part of $\overline{G}_1$ plotted versus Re for $\alpha = 0.3$ and different values of R_d.

after analysing much experimental data of different researchers, proposed

$$\frac{\overline{q^*}}{\omega^* d^{*2}} = \left(\frac{0.2\theta}{f_w}\right)^{3/2} \tag{42}$$

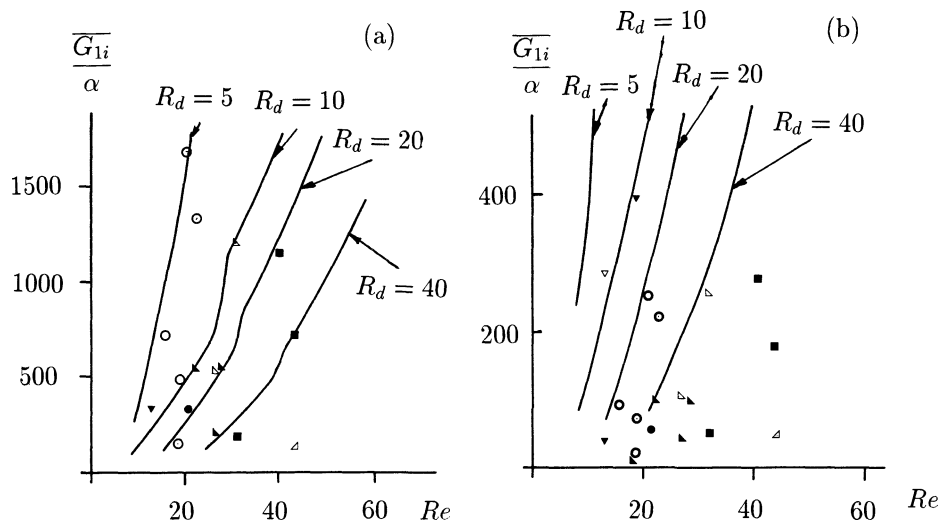

Figure 5. Theoretical and experimental values of $(\overline{G}_{1i}/\alpha_c)$ plotted versus Re. The experimental values are obtained from *table II* evaluating Q by means of both Hallermeier's formula [37] (a) and Sleath's formula [22] (b) (black point = vortex ripple; white point = rolling-grain ripple). ▼, ▽ $5 < R_d < 10$; ●, ○ $10 < R_d < 15$; ▶, ▷ $15 < R_d < 20$; ■, □ $20 < R_d < 25$; ◀, ◁ $25 < R_d < 30$.

while Sleath [33] in his book suggested

$$\frac{\overline{q^*}}{\sqrt{(s-1)gd^{*3}}} \cong 1.95(\theta - \theta_c)^{3/2}. \tag{43}$$

In (42), (43) θ is the Shields parameter defined by

$$\theta = \frac{\tau^*}{(\rho_s^* - \rho^*)g^*d^*}, \tag{44}$$

where τ^* is the maximum bed shear stress and f_w the friction coefficient [38]. The relationship between τ^* and the value of V^* appearing in (12) can be easily obtained by the knowledge of the flow field. Even though for small values of R_d the theory tends to underestimate the migration speed of ripples, while for large values of R_d it tends to overestimate $\overline{G_{1i}}/\alpha$, the trend of the experimental data is well predicted by the analysis and the quantitative agreement between the theoretical predictions and the experimental findings is fair, taking into account the uncertainty in the sediment transport rate formulae which can be appreciated looking at the different predictions which are obtained using Hallermeier or Sleath's formulae. In order to compare the theoretical predictions and the experimental data, the values of the sediment Reynolds number should be carefully considered.

It is also worth noticing that the experimental values of $\overline{G}_{1i}/\alpha$ for vortex ripples (steepness of the bottom profile larger than 0.1) follow the trend of the data for rolling-grain ripples thus showing that, at least for the values of the parameters presently investigated, the migration speed does not depend on the amplitude of the ripples as predicted by the theory. As already pointed out the values of $\overline{G}_{1i}/\alpha$ increase by increasing Re while they decrease when increasing values of R_d are considered. The somewhat discontinuous behaviour of the migration speed of ripples, which appears in *figure 5(a)* for Re approximately equal to 18 (less evident), 28, 32, 40, when R_d is equal to 5, 10, 20, 40 respectively, is related to the discontinuities observed by Blondeaux [11] in the value of the critical wavenumber and have the same physical explanation: during the wave cycle sediments

are subject to the action of a different number of steady recirculating cells depending on the value of s^*/l^* which in turn depends on Re (s^* being the amplitude of water displacement oscillations just outside the bottom boundary layer). When the number of steady recirculating cells which affect the motion of sediment grains changes, a large variation of α_c and of $\overline{G_{1i}}/\alpha_c$ is produced.

4. Conclusion

Ripple formation underneath a sea wave is analysed retaining nonlinear terms in momentum equation to account for the presence of a steady drift. Ripples are thus found to migrate at a constant rate which depends on wave and sediment characteristics. The main assumptions and the limitations of the analysis have been discussed both in the introduction and in Sections 2 and 3. Here we want to remind the reader that the flow regime is assumed laminar and ripples of small amplitude are considered. Therefore the theoretical results described in the paper strictly concern the early stages of ripple formation and the equilibrium configuration of rolling-grain ripples while no theoretical information can be gained on vortex ripples which are characterized by such large amplitudes that flow separation is induced and large vortex structures characterized by a highly nonlinear dynamics are generated. However the comparison of the theoretical results with the experimental data (see *figure 5*) seems to indicate that the theoretical predictions of the migration speed of ripples can be used somewhat beyond the range of the parameters for which they are supposed to be strictly valid. For example the analysis may provide useful information on the migration of vortex ripples, even though these ripples have an amplitude and a wavelength which differ from those predicted by the linear analysis of Blondeaux [11] and weakly nonlinear analysis by Vittori and Blondeaux [15], since the flow field is characterized by strongh nonlinear effects (see [39]). The difficulties of studying the time development of vortex ripples call for a numerical solution and an extension of the works by Sleath [40], Blondeaux and Vittori [41] and Hansen and al. [42] accounting for the presence of a steady drift would be quite useful and would help to understand the basic mechanism of cross-shore sediment transport in that part of the nearshore region characterized by the presence of sea ripples.

At last let us briefly discuss whether the uncertainty in the sediment transport relationship, which may be larger than the perturbation parameters, makes the asymptotic analysis still significant. In order to discuss this point, it is first necessary to point out that the functions describing the x-dependence of the basic state and the x-dependence of the perturbation are orthogonal. Hence the problem describing the propagating sea wave over the cohesionless bottom (the basic state) can be decoupled from that describing the time development of ripples (the perturbation).

First the analysis solves the problem for the sea wave. With the assumptions described in Section 2 the velocity field is solved exactly while the amount of sediment moved by the wave can be quantified only with some uncertainty because the sediment transport predictor is rather simplistic. However the time scales of the hydrodynamic and morphodynamic problems are vastly different and the bottom configuration differs from the flat one by a negligible amount which does not need to be exactly quantified.

Then the analysis tackles the problem for the ripples. The perturbations of the basic flow they induce are determined exactly by assuming the ripple amplitude to be small. The time development of the bottom configuration is then obtained by a sediment balance which provides ordinary differential equations for the amplitudes of the different spatial components of the bed profile. The coefficients of these differential equations are known with some uncertainty because of the uncertainty in the sediment transport predictor. It follows that the predictions of the vertical displacement of the bottom and hence of ripple characteristics are affected by a significant relative error. However the latter cannot be much larger than that affecting the sediment transport predictions. Therefore even though the analysis cannot determine ripple characteristics exactly, it certainly

Table II. Experimental data (d^*, sediment diameter; h^*, water depth; T^*, wave period; $2a^*$, wave height; l^*, ripple wavelength; h_r^*, ripple height; v_r^*, ripple migration speed in the direction of wave propagation; r.g.r. = rolling-grain ripples; v.r. = vortex ripples; $(l_2/l_1 - 1)$, symmetry index).

Experiment No	d^*[mm]	h^*[cm]	T^*[s]	$2a^*$[cm]	l^*[cm]	h_r^*[cm]	v_r^*[cm/s]	ripple type	symmetry index
1	.54	10	2.20	1.08	3.30	0.3	0.048	r.g.r.	
2	.35	10	1.05	1.98	2.25	0.4	0.013	v.r.	
3	.35	10	0.91	3.30	2.35	0.2	0.025	r.g.r.	
4	.35	10	1.25	2.00	2.91	0.5	0.018	v.r.	
5	.35	10	1.10	3.10	3.00	0.4	–.043	v.r.	
6	.54	10	1.50	1.36	1.90	0.2	–.074	v.r.	
7	.54	12	1.50	0.63	2.10	0.2	0.017	r.g.r.	
8	.54	12	1.70	0.69	2.40	0.3	0.066	v.r.	
9	.54	12	2.40	0.69	3.40	0.4	0.012	v.r.	
10	.54	14	1.80	1.06	1.70	0.2	0.051	v.r.	
11	.54	14	2.00	0.49	3.40	0.2	0.016	v.r.	
12	.54	14	2.60	0.85	4.40	0.4	0.081	r.g.r.	
13	.35	15	1.17	5.30	3.39	0.3	–.027	r.g.r.	
14	.35	15	1.30	4.17	3.05	0.4	0.051	v.r.	
15	.35	15	1.23	4.98	4.00	0.5	–.017	v.r.	
16	.35	15	1.57	2.89	3.47	0.7	0.016	v.r.	
17	.35	15	1.17	3.34	3.43	0.4	0.001	v.r.	
18	.35	15	1.86	3.24	3.61	0.8	–.018	v.r.	
19	.35	15	1.70	2.99	3.64	0.9	0.021	v.r.	
20	.35	15	0.80	3.52	2.43	0.2	–.056	r.g.r.	
21	.35	15	0.65	3.49	1.51	0.1	–.030	r.g.r.	
22	.35	15	1.53	2.96	3.74	0.8	0.022	v.r.	
23	.35	15	0.70	3.50	1.79	0.2	–.027	v.r.	
24	.54	16	1.60	0.51	2.00	0.2	0.010	r.g.r.	
25	.54	16	1.80	0.47	2.70	0.2	0.045	v.r.	
26	.54	16	2.20	0.71	3.40	0.1	0.056	r.g.r.	
27	.54	18	3.00	0.79	4.00	0.8	0.013	v.r.	
28	.54	18	2.20	0.73	3.40	0.5	0.012	v.r.	
29	.54	18	3.50	0.49	5.30	0.8	0.010	v.r.	
30	.54	18	4.00	0.40	5.40	0.79	0.000	v.r.	0.182
31	.54	20	2.60	0.66	4.40	0.4	0.025	r.g.r.	
32	.54	20	2.00	0.72	2.40	0.2	0.016	r.g.r.	
33	.54	20	3.80	1.14	5.50	0.8	0.025	v.r.	
34	.54	20	3.40	1.14	6.10	1.0	0.050	v.r.	
35	.54	20	3.00	2.20	4.44	0.47	0.012	v.r.	0.130
36	.54	20	3.80	1.20	4.00	0.66	0.010	v.r.	0.125
37	.54	22	2.20	1.01	3.00	0.2	0.033	r.g.r.	
38	.54	22	1.10	1.19	1.60	0.1	0.016	r.g.r.	
39	.54	22	1.20	1.20	1.69	0.11	0.016	r.g.r.	0.225
40	.54	22	1.25	1.30	1.60	0.16	–.008	r.g.r.	0.303
41	.54	22	1.40	1.50	1.90	0.13	0.018	r.g.r.	0.076
42	.54	22	1.25	1.40	1.55	0.11	0.019	r.g.r.	0.192

helps to understand the processes leading to ripple formation and development. Moreover the analysis indicates the dimensionless parameters controlling ripple characteristics (a.o. ripple wavelength, ripple migration speed) and suggests some possible relationships.

Appendix A: The experiments

The experiments were performed in a wave channel 8 m long, 0.5 m wide and 0.7 m deep. Waves were generated at one end of the channel by a piston type wave-maker and were absorbed at the other end by a beach of small gravel with a constant slope of 20%. To decrease wave harmonics, filters consisting of wire-net cylinders were situated near the wave-maker. In the central part of the channel a 6 m long sediment bed was created, beginning about 1 m downwave from the wave-maker. The bed was 3 cm thick. The height of the surface waves was measured by means of a resistance gauge and by a pointer while their period was fixed by an electronic device which controlled the stepping motor moving the wave maker. When ripples appeared, their geometrical characteristics (wavelength, height, symmetry index) were measured by means of a pointer averaging over ten ripples. The symmetry index of ripples is defined as the ratio between the distance l_2 of a crest from the following trough and the distance l_1 of the same crest from the preceding trough. Because of the roughness induced by sediment grains, it was difficult to locate the troughs and the crests of the ripples. For this reason only a few measurements of l_2/l_1 were made. Moreover large errors should be expected. The propagation speed was estimated measuring the distance covered by a ripple crest during a fixed time interval (about two minutes). Two bed materials were used: plastic particles having a density ρ_s equal to 1050 kg/m^3 and a median diameter equal to 0.35 mm and 0.54 mm respectively. A sieve analysis showed that both the materials were well sorted. Plastic particles were used instead of sand because our mobile wave-maker does not allow large amplitude waves to be generated, able to move heavy particles.

Before each experiment, the bed was smoothed by dragging a screen over the sediment surface. Then the waves were generated until the resulting ripples on the bed attained constant and uniform height and length and a steady rate of advance. The migration speed was then measured and eventually the wave-maker was stopped and the geometrical ripple characteristics measured. The data obtained are summarized in *table II* where the observed ripples are classified as rolling-grain ripples (r.g.r.) or vortex ripples (v.r.) according to the criterion proposed by Sleath [22]: rolling-grain ripples are characterized by values of h_r^*/l^* smaller than 0.1 while vortex ripples by values of h_r^*/l^* larger than 0.1.

Acknowledgements

The authors wish to thank Ing. Veronica Galletta who assisted them in performing some of the experiments described in Appendix A.

This research has been partly supported by the Office of Naval Research (O.N.R.) under contract n. N00014-97-1-0790, by the EU under contract n. MAS3-CT97-0115 ‘SEDMOC’ in the framework of the Marine Science and Technology Programme (MAST-III) and by the Ministero dell’Università e della Ricerca Scientifica e Tecnologica.

References

[1] Allen J.R.L., Developments in Sedimentology, Elsevier, 1984.
[2] Inman D.L., Tech. Mem. U.S. Beach Erosion, No. 100, 1957.

[3] Inman D.L., Bowen A.J., Flume experiments on sand transport by waves and currents, Proc. 8th Conf. Coastal Eng., 1963, pp. 137–150.
[4] Harms J.C., Hydraulic significance of some sand ripples, B. Geol. Soc. Am. 80 (1969) 363–396.
[5] Tanner W.F., Numerical estimates of ancient waves, water depth and fetch, Sedimentology 16 (1971) 71–88.
[6] Tietze K.W., Private communication to J.R.L. Allen, 1979.
[7] Allen J.R.L., A model for the interpretation of wave ripple-marks using their wavelength, textural composition and shape, J. Geol. Soc. Lond. 136 (1979) 673–683.
[8] Gilbert G.K., Ripple marks, Science 3 (1884) 375–376.
[9] Gilbert G.K., Ripple marks and cross-bedding, B. Geol. Soc. Am. 10 (1899) 135–140.
[10] Stone R.O., Summers H.J., Study of subacqueous and subaerial sand ripples, Univ. S. Calif. Dep. Geol. Sci. Final rep. 72-1, 1972.
[11] Blondeaux P., Sand ripples under sea waves. Part 1. Ripple formation, J. Fluid Mech. 218 (1990) 1–17.
[12] Blondeaux P., Vittori G., Vorticity dynamics in an oscillatory flow over a rippled bed, J. Fluid. Mech. 226 (1991) 257–289.
[13] Hara T., Mei C.C., Oscillating flows over periodic ripples, J. Fluid Mech. 211 (1990) 183–209.
[14] Hara T., Mei C.C., Centrifugal instability of an oscillatory flow over periodic rippples, J. Fluid Mech. (1990) 217 1–32.
[15] Vittori G., Blondeaux P., Sand ripples under sea waves. Part 2. Finite amplitude development, J. Fluid Mech. 218 (1990) 19–39.
[16] Vittori G., Blondeaux P., Sand ripples under sea waves. Part 3. Brick-pattern ripple formation, J. Fluid Mech. 239 (1992) 23–45.
[17] Hara T., Mei C.C., Shum K.T., Oscillating flow over periodic ripples of finite slope, Phys. Fluids 4 (1992) 1373–1384.
[18] Lyne W.H., Unsteady viscous flow over a wavy wall, J. Fluid Mech. 50 (1971) 33–48.
[19] Sleath J.F.A., On rolling-grain ripples, J. Hydraul. Res. 14 (1976) 69–81.
[20] Kennedy J.F., Falcon M., Wave-generated sediment ripples, Rep. n. 86, Dept. of Civil Engineering, MIT, U.S., 1965.
[21] Foti E., Blondeaux P., Sea ripple formation: the turbulent boundary layer case, Coastal Eng. 25 (1995) 227–236.
[22] Sleath J.F.A., Sea Bed Mechanics, Wiley, 1984.
[23] Fredsøe J., Deigaard R., Mechanics of Coastal Sediment Transport, World Scientific, 1992.
[24] Nielsen P., Coastal Bottom Boundary Layers and Sediment Transport, World Scientific, 1992.
[25] Blondeaux P., Vittori G., Boundary layer and sediment dynamics under sea waves, in: Liu P.L.F. (Ed.), Advances in Coastal and Ocean Engineering, Vol. 4, World Scientific, 1999, pp. 133–190.
[26] Vittori G., Blondeaux P., Mass transport under sea waves over a rippled bed, J. Fluid Mech. 314 (1996) 247–265.
[27] Sleath J.F.A., Sea bed boundary layers, in: Le Méhauté, Hanes (Eds), The Sea, Wiley, 1990.
[28] Sleath J.F.A., Velocity measurements close to bed in a wave tank, J. Fluid Mech. 42 (1970) 111–123.
[29] Grass J.A., Ayoub N.M., Bed load transport of fine sand by laminar and turbulent flow, in: Edge B.L. (Ed.), Proc. 18th Coastal Engineering Conference, 1982, pp. 1589–1599.
[30] Wen J., Liu P.L.F., Mass transport under partially reflected waves in a rectangular channel, J. Fluid Mech. 266 (1994) 121–145.
[31] Longuet-Higgins M.S., Mass transport in water waves, Philos. T. Roy. Soc. 345 (1953) 535–581.
[32] Engelund F., Flow and bed topography in channel bends, J. Hydraul. Eng.-ASCE 160 (HY 11) (1974) 1631–1648.
[33] Sleath J.F.A., Measurements of bed load in oscillatory flow, J. Waterw. Port C-ASCE 104 (WW3) (1978) 291–307.
[34] Fredsøe J., On the development of dunes on erodible channels, J. Fluid Mech. 64 (1974) 1–16.
[35] Kaneko A, Honji H., Double structures of steady streaming in the oscillatory viscous flow over a wavy wall, J. Fluid Mech. 93 (1979) 727–736.
[36] Gray C., Fredsøe J., Deigaard R., Flume experiments on bed wave shape and sand transport by currents and waves, Prog. Rep., Tech. Univ. Denmark, 73, 1991, pp. 7–20.
[37] Hallermeier R.J., Oscillatory bedload transport: data review and simple formulation, Cont. Shelf Res. 1 (1982) 159–190.
[38] Jonsson I.G., Measurements in the turbulent wave boundary layer, in: Proc. 10th Congr. Int. Ass. Hydraul. Res., Vol 1, 1963, pp. 85–92.
[39] Andersen K.H., The dynamics of ripples benehat surface waves and topics in shell models of turbulence, Ph.D. Thesis, Niels Bohr Institute, University of Copenhagen, ISVA-Technical University of Denmark, 1999.
[40] Sleath J.F.A., A numerical study of the influence of bottom roughness on mass transport by water waves, in: Proc. Int. Conf. Num. Methods in Fluid Dynamics, Southampton, U.K., 1973.
[41] Blondeaux P., Vittori G., Oscillatory flow and sediment motion over a rippled bed, in: Proc. 22 Conf. Coastal Eng., 1990, pp. 2186–2199.
[42] Hansen E.A., Fredsøe J., Deigaard R., Distribution of suspended sediment over wave.generated ripples, J. Waterw. Port C-ASCE 120 (1) (1994) 37–55.